Available online at www.sciencedirect.com
SCIENCE DIRECT®
Journal of Catalysis 224 (2004) 370–383
JOURNAL OF CATALYSIS
www.elsevier.com/locate/jcat

Isotopic and kinetic assessment of the mechanism of reactions of CH_4 with CO_2 or H_2O to form synthesis gas and carbon on nickel catalysts

Junmei Wei and Enrique Iglesia *

Department of Chemical Engineering, University of California at Berkeley, Berkeley, CA 94720, USA

Received 24 November 2003; revised 16 February 2004; accepted 24 February 2004

Available online 20 April 2004

Abstract

Kinetic and isotopic measurements for catalysts and conditions that rigorously excluded transport and thermodynamic artifacts led to a common sequence of elementary steps for reactions of CH_4 with CO_2 or H_2O and for its stoichiometric decomposition on Ni/MgO catalysts. Turnover rates for forward reactions of CH_4/CO_2 and CH_4/H_2O mixtures were proportional to CH_4 pressure (5–450 kPa) and independent of the partial pressure of the CO_2 or H_2O coreactants (5–450 kPa). These turnover rates and their first-order rate constants and activation energies are also similar to those measured for CH_4 decomposition, indicating that these reactions are mechanistically equivalent and that C–H bond activation is the sole kinetically relevant step in all three reactions. These conclusions were confirmed by identical CH_4/CD_4 kinetic isotope effects ($k_H/k_D = 1.62$–1.71) for reforming and decomposition reactions and by undetectable H_2O/D_2O isotopic effects. The kinetic relevance of C–H bond activation is consistent with the relative rates of chemical conversion and isotopic mixing in a $CH_4/CD_4/CO_2$ mixture and with the isotopic evidence for the quasi-equilibrated nature of coreactant activation and H_2 and H_2O desorption obtained from reactions of $CH_4/CO_2/D_2$ and $^{12}CH_4/^{12}CO_2/^{13}CO$ mixtures. These quasi-equilibrated steps lead to equilibrated water–gas-shift reactions during CH_4 reforming, a finding confirmed by measurements of the effluent composition. These elementary steps provide also a predictive model for carbon filament growth and identify a rigorous dependence of the carbon thermodynamic activity on various kinetic and thermodynamic properties of elementary steps and on the prevalent concentrations of reactants and products, specifically given by $P_{CH_4}P_{CO}/P_{CO_2}$ (or $P_{CH_4}P_{H_2}/P_{H_2O}$) ratios. These mechanistic features on Ni surfaces resemble those previously established for supported noble metal catalysts (Rh, Pt, Ir, Ru). These direct measurements of C–H bond activation turnover rates allowed the first direct and rigorous comparison of the reactivity of Ni and noble metal catalysts for CH_4-reforming reactions, under conditions of strict kinetic control and relevant commercial practice and over a wide range of compositions and metal dispersions.

Keywords: C–H bond activation; Methane reforming; Carbon filaments; Nickel catalysts; Isotopic tracer methods

1. Introduction

CH_4 reactions with CO_2 or H_2O on Group VIII metals form synthesis gas precursors to valuable fuels and chemicals, as first shown by Fischer and Tropsch [1]. Industrial practice relies on Ni catalysts, because of cost and availability concerns about noble metals. Ni-based catalysts tend to form unreactive carbon residues that block active sites and catalyst pores, and which lead ultimately to the formation of carbon filaments and to the elution of Ni crystallites from catalyst pellets and reactors [2–4]. Carbon filament formation pathways are also of significant interest for the on-purpose synthesis of carbon nanotubes catalyzed by metal particles [5–7]. Detailed molecular-level pathways for conversion of CH_4 to H_2/CO mixtures and carbon, and even their kinetic response to reactant concentrations, remain controversial and often contradictory, even after many studies [8–28]. Kinetic measurements are often corrupted by ubiquitous concentration and temperature gradients at the high temperatures required for these endothermic reactions, which require the activation of strong C–H bonds, and by significant but often unrecognized contributions from reverse reactions as reactions approach equilibrium.

The prevailing controversies are illustrated by the broad range of disparate rate equations for CH_4 reforming shown in Table 1. For instance, a complex rate equation, purported to resolve previous contradictory results on Ni-based cata-

* Corresponding author. Fax: +510 642 4778.
E-mail address: iglesia@cchem.berkeley.edu (E. Iglesia).

0021-9517/$ – see front matter
doi:10.1016/j.jcat.2004.02.032

Table 1
Proposed rate expressions for CH_4-reforming reactions on Ni-based catalysts

Rate expression	Coreactant	Catalyst	Refs.
$r = kP_{CH_4}$	H_2O	Ni/Kieselguhr	[8]
$r = \frac{kP_{CH_4}}{1 + a[P_{H_2O}/P_{H_2}] + bP_{CO}}$	H_2O	Ni foil	[9]
$r = a/P_{CH_4}^{2.5}(P_{CH_4}P_{H_2O} - P_{CO}P_{H_2}^3/b)/\alpha^2 + c/P_{CH_4}^{2.5}(P_{CH_4}P_{H_2O} - P_{CO}P_{H_2}^3/d)/\alpha^2$	H_2O	$Ni/MgAl_2O_4$	[13,14][a]
$r = \frac{aP_{CH_4}P_{CO_2}}{bP_{CO}P_{H_2}^{(4-x)/2} + (1 + cP_{CH_4})P_{CO_2}}$	CO_2	Ni/TiO_2, Ni/MgO, Ni/SiO_2	[16]
$r = \frac{kP_{CH_4}P_{CO_2}}{(1 + K_{CH_4}P_{CH_4})(1 + K_{CO_2}P_{CO_2})}$	CO_2	Ni/Al_2O_3, Ni/CeO_2–Al_2O_3	[20]
$r = \frac{aP_{CH_4}P_{CO_2}}{bP_{CH_4}P_{CO_2} + cP_{CH_4} + dP_{CO}}$	CO_2	Ni/La_2O_3	[23]

[a] $\alpha = 1 + K_{CO}P_{CO} + K_{H_2}P_{H_2} + K_{CH_4}P_{CH_4} + K_{H_2O}P_{H_2O}/P_{H_2}$.

lysts [13,14],

$$r_{CH_4} = \frac{a}{P_{H_2}^{2.5}}\left(P_{CH_4}P_{H_2O} - \frac{P_{H_2}^3 P_{CO}}{b}\right)\Big/[\alpha]^2 + \frac{c}{P_{H_2}^{3.5}}\left(P_{CH_4}P_{H_2O}^2 - \frac{P_{H_2}^4 P_{CO_2}}{d}\right)\Big/[\alpha]^2, \quad (1)$$

$$[\alpha] = [1 + K_{CO}P_{CO} + K_{H_2}P_{H_2} + K_{CH_4}P_{CH_4} + K_{H_2O}P_{H_2O}/P_{H_2}],$$

and widely used [29,30], predicts infinite rates at the reactor inlet and substantial surface coverages by chemisorbed O atoms and by molecularly adsorbed H_2, CH_4, and CO at temperatures well above those required for their desorption or dissociation. CO_2 reforming of CH_4 was proposed to occur via reversible CH_4 and CO_2 dissociation to form CH_xO [16] as the most abundant reaction intermediate, and CH_4 activation and CH_xO decomposition as kinetically relevant steps to give the rate equation:

$$r = \frac{aP_{CH_4}P_{CO_2}}{bP_{CO}P_{H_2}^{(4-x)/2} + (1 + cP_{CH_4})P_{CO_2}}. \quad (2)$$

These conflicting rate equations and reaction pathways led us to collect and interpret kinetic data that rigorously exclude transport and thermodynamic artifacts and to carry out isotopic studies to probe the reversibility and kinetic relevance of specific elementary steps. In doing this, we have developed a unified treatment of CH_4 reactions with H_2O or CO_2, CH_4 decomposition, and water–gas-shift reactions, as well as mechanism-based rate equations for CH_4-reforming reactions. Here, we postulate and confirm via independent measurements a catalytic sequence that reveals a rigorous and intrinsic kinetic and mechanistic equivalence among these reactions. We also provide rigorous evidence for the sole kinetic relevance of C–H bond activation steps and for the equilibrated nature of all elementary steps involved in water–gas-shift catalytic sequences. These elementary steps and their kinetic relevance resemble those recently demonstrated also on noble metal catalysts [31–34], attesting to the generality of the kinetic conclusions. These steps also provide a rigorous and accurate kinetic framework for dynamic treatments of carbon deposition and filament formation during high-temperature CH_4-reforming and decomposition reactions on Ni crystallites [35]. Finally, we report here the first rigorous comparison of CH_4-reforming turnover rates on Ni and noble metal (Pt, Ir, Rh, Ru) surfaces under demonstrated kinetic control, corrected for approach to equilibrium, and under conditions of relevant industrial practice.

2. Experimental methods

Ni/MgO-A (7 and 15 wt%) and Ni/MgO-B (7 wt%) were prepared by incipient wetness impregnation of MgO-A (prepared as described below) or MgO-B (Alfa, CAS 1309-48-4) with an aqueous $Ni(NO_3)_2 \cdot 6H_2O$ (Alfa, 99.9%) solution and subsequent drying at 393 K in ambient air and treatment in flowing dry air (Airgas, UHP, 1.2 $cm^3/(g\,s)$) as the temperature was increased at 0.167 K/s to 923 K and held for 5 h. Samples were then treated in H_2 (Airgas, UHP, 50 $cm^3/(g\,s)$) by heating to 1123 K at 0.167 K/s and holding for 3 h. MgO-A powders were prepared by sol–gel methods using supercritical drying, a procedure that leads to MgO-A crystallites of small and uniform diameter and to high ultimate dispersion of Ni metal clusters [36]. In this sol–gel method, $Mg(OH)_2$ was first obtained by hydrolysis of 0.4 M aqueous $MgCl_2$ (Aldrich, > 98 wt%) at pH 10, maintained by controlled addition of 14.8 M NH_4OH. Precipitates were filtered and washed with deionized water until Cl ions were no longer detected in the eluted water using $AgNO_3$ ($Cl^- <$ 10 ppm). Powders were then washed three times with anhydrous ethanol (10 cm^3/g-MgO), with acetone, which is very soluble in liquid CO_2, and then with liquid CO_2 within a supercritical dryer, where they were heated to 311–313 K at 0.008 K/s while the CO_2 pressure was increased to 8.2–8.9 MPa to reach the critical point (304.5 K, 7.6 MPa). The pressure was then released to vaporize CO_2 directly from its supercritical state and the sample treated at 923 K for 3 h in flowing dry air (Airgas, UHP, 1.2 $cm^3/(g\,s)$) by heating

at 0.167 K/s. Synthesis procedures for the supports used for Ru [31], Pt [32], Ir [33], and Rh [34] catalysts and their synthesis procedures have been reported elsewhere.

Reduction studies of supported NiO precursors were carried out in a Quantasorb analyzer (Quantachrome Corporation) using thermal conductivity detection, electronic mass-flow controllers, a programmable furnace, and on-line molecular sieve traps to remove the water formed during reduction. Samples (0.1 g) were reduced in 20% H_2/Ar (0.67 cm^3/s, Matheson UHP, certified mixture) as the temperature increased to 1123 K at 0.167 K/s. The thermal conductivity response was calibrated using CuO reduction (Aldrich, 99.995%).

Ni metal dispersion was measured on fresh samples from uptakes of strongly chemisorbed H_2 at 313 K (3–50 kPa) using a Quantasorb chemisorption analyzer (Quantachrome Corp.), after reducing samples ex situ at 1123 K for 3 h and then at 873 K for 0.5 h within the adsorption cell. A backsorption isotherm was measured by repeating this procedure after evacuation at 313 K for 0.5 h. The difference between chemisorption and backsorption isotherms was used to measure strongly chemisorbed hydrogen uptakes; Ni dispersion was calculated using 1:1 H:Ni titration stoichiometry [16].

Rates of CH_4–CO_2 and CH_4–H_2O reforming and of CH_4 decomposition were measured on catalyst pellets (250–425 μm) diluted with inert γ-Al_2O_3 powders (5/25 mg); these pellets were then mixed with acid-washed quartz powder (500 mg; 250–425 μm) in packed catalyst beds. CO_2- and H_2O-reforming rates were measured at 823–1023 K and 100–1500 kPa total pressure using a microreactor system previously described [31]. Reactant concentrations were independently varied using 50% CH_4/Ar (Matheson UHP) and 50% CO_2/Ar (Matheson UHP) certified mixtures (metered by electronic controllers) and a pure H_2O stream (introduced with a syringe pump; ISCO Model 500D). All transfer lines after H_2O introduction were kept at 500 K to avoid condensation. Reactant and product concentrations were measured with a Hewlett-Packard 6890 gas chromatograph using a Carboxen 1000 packed column (3.2 mm × 2 m) and thermal conductivity detection.

CH_4 and CD_4 decomposition rates on 7 wt% Ni/MgO-A were measured from dihydrogen and methane isotopomer concentrations by mass spectrometry (Leybold Inficon, Transpector Series). Reactant mixtures were prepared from 50% CH_4/Ar (Matheson, certified mixture) or CD_4 (Isotec, chemical purity > 99.0%) and Ar (Airgas, UHP). CH_4 and CD_4 mass fragments at 15 and 18 amu were used to measure their respective concentrations, and 2 and 4 amu were used for H_2 and D_2, respectively. Decomposition rates were extrapolated to the time of initial contact with methane to obtain initial rates before significant carbon formation. Rate constants were obtained from reaction rates using the observed linear dependence of decomposition rates on CH_4 pressure.

Isotopic tracer studies on 7 wt% Ni/MgO-A were carried out using a transient flow apparatus with short hydrodynamic delays (< 5 s). Chemical and isotopic compositions were measured by mass spectrometric analysis of the reactor effluent (Leybold Inficon, Transpector Series). CD_4 (Isotec, chemical purity > 99.0%), D_2O (Isotec, chemical purity > 99.0%), and 5% D_2/Ar and ^{13}CO (Isotec, chemical purity > 99.0%) were used as reactants. Intensities at 15 and 17–20 amu were used to measure methane isotopomer concentrations. CH_4 and CD_4 standard fragmentation patterns were measured, and those for CHD_3, CH_2D_2, and CH_3D were calculated using reported methods [37]. Intensities at 18, 19, and 20 amu were used to determine water isotopomers and those at 28, 29, 44, and 45 amu to measure ^{12}CO, ^{13}CO, $^{12}CO_2$, and $^{13}CO_2$ concentrations, respectively.

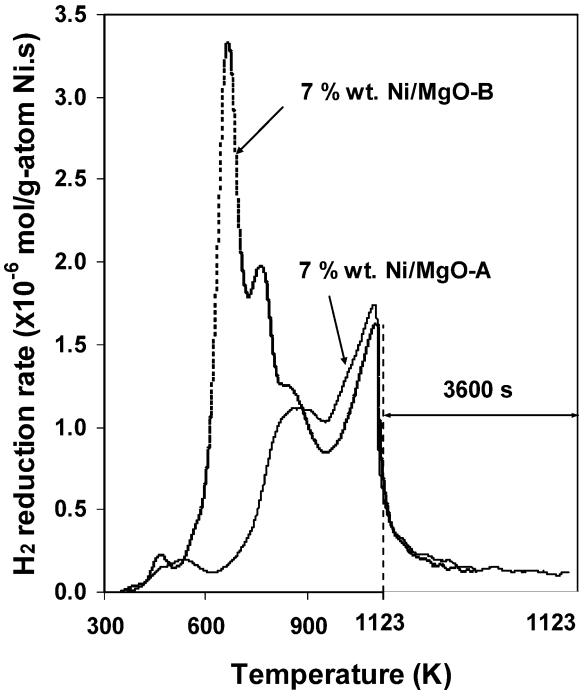

Fig. 1. TPR profile of 7 wt% Ni/MgO-A and Ni/MgO-B (100 mg catalyst, 20% H_2/Ar at 0.67 cm^3/s, temperature increased to 1123 K at 0.167 K/s).

Carbon formation rates were measured during CH_4 reforming at 873 K using a tapered-element oscillating quartz element (Ruprecht & Patashnick, 1500 pma) microbalance while continuously monitoring the effluent by mass spectrometry. Samples (30 mg) were reduced at 1123 K for 3 h and then again within the balance chamber at 873 K for 0.5 h.

3. Results and discussion

3.1. Catalyst characterization

Fig. 1 shows reduction rates for 7 wt% Ni/MgO-A and 7 wt% Ni/MgO-B in H_2 during temperature ramping. The reduction profile of 15 wt% Ni/MgO-A is similar to that of 7 wt% Ni/MgO-A. Only ∼ 28.2, 46.3, and 43.4% of the Ni atoms in the samples are reduced to Ni^0 after treatment at 1123 K for 7 wt% Ni/MgO-A, 15 wt% Ni/MgO-A,

Table 2
Extent of reduction, dispersion, and average crystal size for Ni/MgO catalysts

Catalyst	Percentage reduction (%)[a]	Dispersion (%)[b]	Average particle size (nm)[c]
7 wt% Ni/MgO-A	28.2	14.8	6.7
15 wt% Ni/MgO-A	46.3	9.6	10.4
7 wt% Ni/MgO-B	43.4	9.3	10.8

[a] The fraction of the reduced Ni atoms to the total Ni atoms.
[b] The fraction of the surface Ni atoms from H_2 chemisorption to the reduced Ni atoms.
[c] Estimated from fraction Ni dispersion using $D = 1/d$ [38].

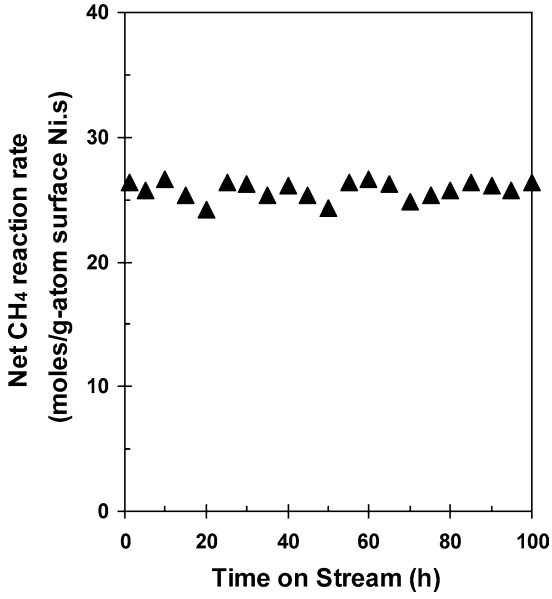

Fig. 2. Net CH_4 reaction rate for H_2O–CH_4 reaction as a function of time on stream on 7 wt% Ni/MgO-A (973 K, 33 kPa CH_4, 33 kPa H_2O, balance Ar, $\eta = 0.2$).

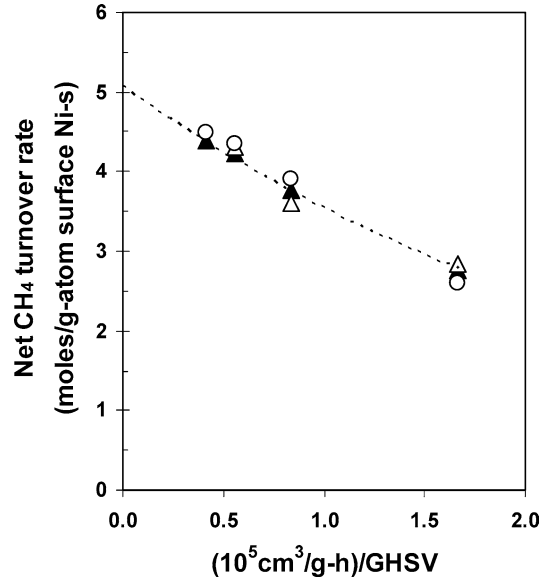

Fig. 3. Net CH_4 turnover rates versus residence time for CH_4–H_2O reaction on 7 wt% Ni/MgO-A at 873 K ((○) 10 mg catalyst diluted with 100 mg Al_2O_3 within pellets, then diluted with 500 mg ground quartz, pellet size 250–425 μm; (▲) 10 mg catalyst diluted with 50 mg Al_2O_3 within pellets, then diluted with 500 mg ground quartz, pellet size 250–425 μm; (△) 10 mg catalyst diluted with 50 mg Al_2O_3 within pellets, then diluted with 500 mg ground quartz, pellet size 63–106 μm, extrapolation of the dash line to zero residence time gives forward CH_4 turnover rate).

and 7 wt% Ni/MgO-B, respectively, while the remaining Ni atoms remain unreduced within NiO–MgO solid solutions [38,39]. The number of exposed Ni surface atoms in these three reduced samples is reported as their fractional dispersion in Table 2, defined as the number of exposed Ni atoms, measured by H_2 chemisorption, divided by the number of reduced Ni atoms.

3.2. Kinetic dependence of forward CH_4 reaction rates on reactant and product concentrations

CH_4 reaction rates were measured on Ni/MgO catalysts in the absence of detectable deactivation and of transport or thermodynamic corruption of rate measurements. For 7 wt% Ni/MgO-A, all kinetic measurements were carried out at effluent $P_{CH_4}P_{CO}/P_{CO_2}$ ratios below 4 kPa, which as shown later, led either to undetectable or to catalytically irrelevant carbon formation rates.

Fig. 2 shows CH_4 reaction rates during H_2O–CH_4 reactions at 973 K as a function of time on stream on 7 wt% Ni/MgO-A. CH_4 reaction rates remained constant for 100 h. Transport artifacts were ruled out by dilution of the catalyst pellet with inert Al_2O_3 and dilution of the catalyst bed with ground quartz. The absence of intraparticle and bed transport artifacts was confirmed by similar CH_4–CO_2 reaction rates measured as the pellet size (250–425 vs 63–106 μm) or the extent of dilution within pellets (5:1 to 10:1) was varied (Fig. 3). Fig. 3 shows net CH_4 turnover rates (normalized by exposed Ni atoms) for CH_4–CO_2 reactions at 873 K as a function of residence time. Residence time effects on CH_4 turnover rates reflect reactant depletion and the approach to thermodynamic equilibrium for reforming reactions. Forward reforming rates can be rigorously obtained from measured net rates using an approach to equilibrium parameter (η) evaluated from CH_4–CO_2 and CH_4–H_2O thermodynamic reaction data [40] and measured reactant and product partial pressures:

$$\eta_1 = \frac{[P_{CO}]^2[P_{H_2}]^2}{[P_{CH_4}][P_{CO_2}]}\frac{1}{K_{EQ1}}, \tag{3}$$

$$\eta_2 = \frac{[P_{CO}][P_{H_2}]^3}{[P_{CH_4}][P_{H_2O}]}\frac{1}{K_{EQ2}}. \tag{4}$$

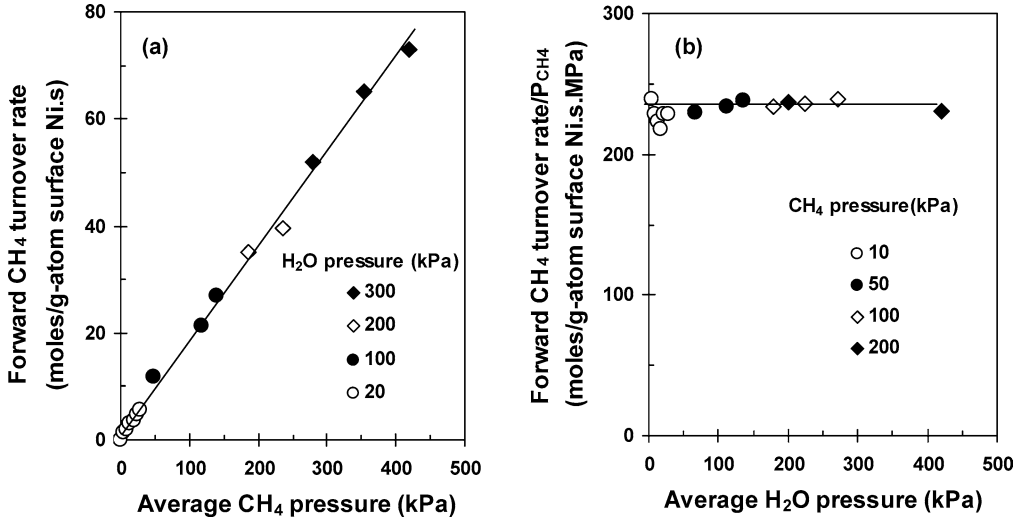

Fig. 4. Effect of CH_4 (a) and H_2O (b) partial pressure on forward CH_4 reaction rate for CH_4–H_2O reaction on 7 wt% Ni/MgO-A (873 K, balance He, average pressure is the average of inlet and outlet pressures of the reactor).

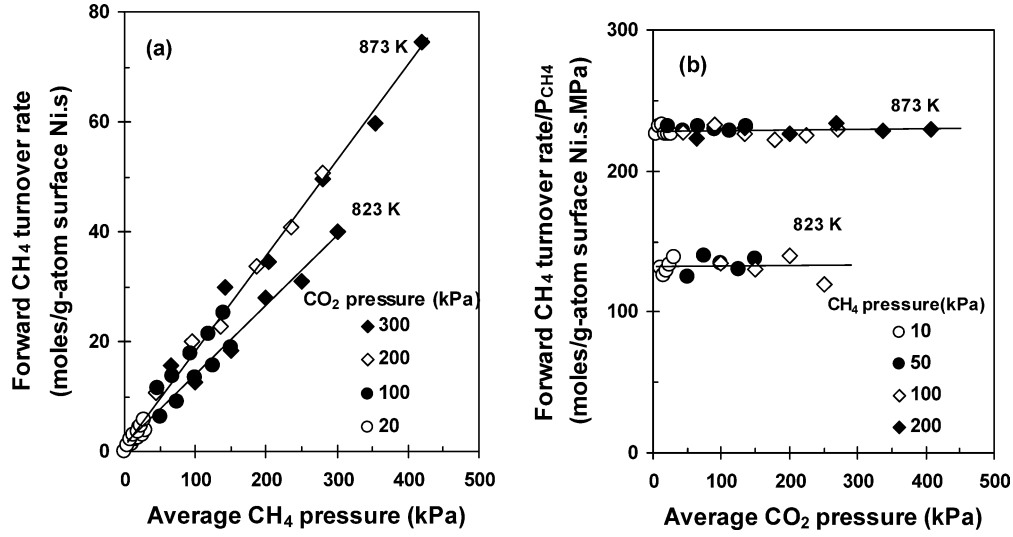

Fig. 5. Effects of CH_4 (a) and CO_2 (b) partial pressure on forward CH_4 reaction rate for CO_2 reforming of CH_4 on 7 wt% Ni/MgO-A (balance He, average pressure is the average of inlet and outlet pressures of the reactor).

In these expressions, $[P_j]$ is the average partial pressure of species j (in atm); it is also used to correct for reactant depletion. K_{EQ1} and K_{EQ2} are equilibrium constants for CH_4–CO_2 and CH_4–H_2O reactions, respectively; η values ranged from 0.05 to 0.20 in this study. Forward turnover rates (r_f) are given by [41]

$$r_f = r_n/(1-\eta), \tag{5}$$

where r_n is the net CH_4 conversion turnover rate. The curve shown in Fig. 3 represents rates predicted from this expression and the first-order dependence of reaction rates on CH_4 concentration reported below.

CH_4–H_2O reaction rates at 873 K and CH_4–CO_2 reaction rates at 823 and 873 K and 100–1500 kPa total reactant pressures are shown as a function of CH_4 and coreactant pressures in Figs. 4 and 5, respectively. For both reactions, forward CH_4 reaction rates increased linearly with increasing CH_4 pressure (5–450 kPa, Figs. 4a and 5a), but they were not influenced by H_2O or CO_2 pressures (5–450 kPa, Fig. 4b). Figs. 4 and 5 also show that forward CH_4 turnover rates using CO_2 and H_2O coreactants are identical to each other within experimental accuracy at any given CH_4 pressure. These rates also resemble initial CH_4 decomposition rates (Table 2, Fig. 6).

H_2 (0–20 kPa) and CO (0–10 kPa) products added to CH_4–CO_2 or CH_4–H_2O reactant mixtures influenced net CH_4 conversion rates at 873 K, but forward rates were unaffected (Fig. 7), indicating that H_2 and CO influenced only the extent to which reforming reactions approach equilibrium, but not the kinetics of forward CH_4-reforming reactions. Thus, previously reported inhibition of CH_4 reaction rates by products may reflect unrecognized contributions from

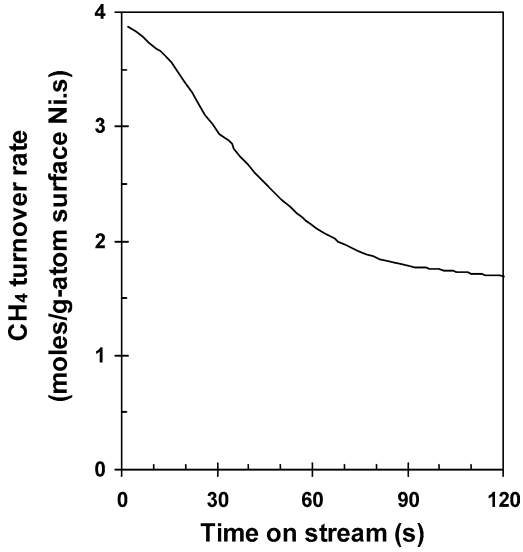

Fig. 6. CH_4 decomposition rate as a function of time on stream on 7 wt% Ni/MgO-A (873 K, 20 kPa CH_4, 100 kPa total pressure, balance Ar).

reverse reaction rates [9,17,22]. CO adsorption enthalpies are 135 kJ/mol at low coverages (< 0.02) and much lower at higher coverages on Ni(100) [42]. These adsorption enthalpies indicate that CO coverages should be well below 0.01 monolayer at 873 K and even at equilibrium CH_4 conversions. The lower adsorption enthalpies typically reported for H_2 (92 kJ/mol [43]) would make hydrogen coverages even lower than for CO. Thus, competitive adsorption is unlikely to influence the availability of metal sites for CH_4 activation and reported inhibition effects predominately reflect contributions from reverse reactions.

These kinetic responses to reactant and product concentrations are consistent with rate-determining CH_4 activation steps on surfaces essentially free of reactive intermediates or coadsorbed products. CH_4-derived chemisorbed intermediates appear to be readily removed via reactions with CO_2 or H_2O coreactants; as a result, the identity and concentration of coreactants become kinetically irrelevant and forward rate data for both CH_4–CO_2 and CH_4–H_2O reactions are accurately described by

$$r_f = kP_{CH_4}, \tag{6}$$

with similar rate constants for the two coreactants (Table 3) and even for stoichiometric CH_4 decomposition reactions. These results and conclusions are similar for the three Ni catalysts in this study and for a wide range of reaction conditions relevant to industrial practice (823–1023 K; 5–450 kPa CH_4, CO_2, or H_2O pressures). The similar rate constants

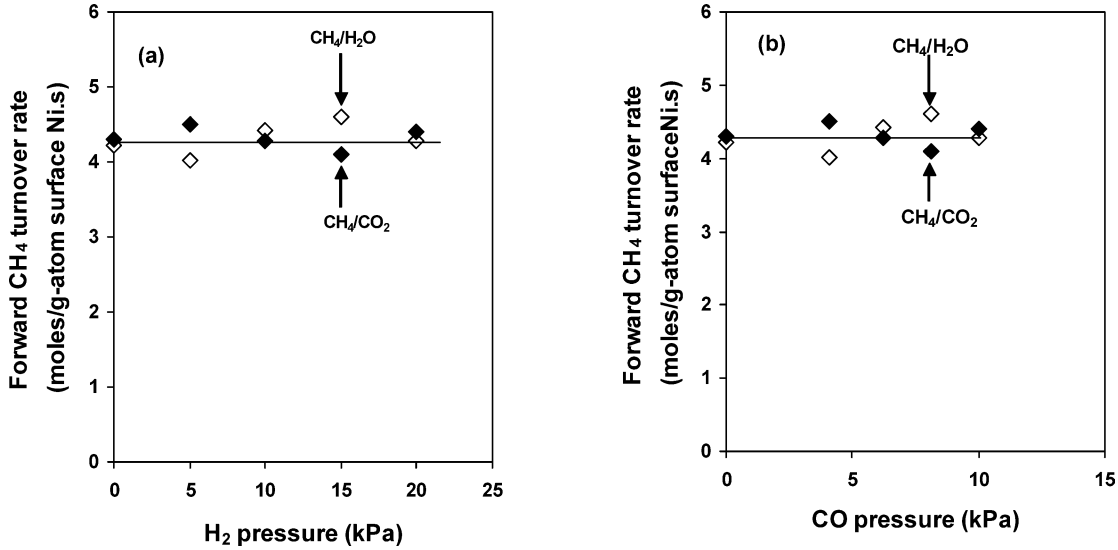

Fig. 7. Effect of H_2 (a) and CO (b) partial pressures on forward CH_4 reaction rate for CH_4-reforming reactions on 7 wt% Ni/MgO-A (873 K, 20 kPa CH_4, 20 kPa CO_2 or H_2O, 100 kPa total pressure, balance He).

Table 3
Forward CH_4 reaction rates, rate constants, preexponential factors, activation energies, and kinetic isotopic effect (KIE) for CH_4 reactions on 7 wt% Ni/MgO-A (873 K, 20 kPa CH_4, 25 kPa CO_2 or H_2O, 100 kPa total pressure, balance Ar)

Coreactant	Turnover rate (s^{-1})	Rate constant (s^{-1} kPa^{-1})	Activation energy (kJ/mol)	Preexponential factor (s^{-1} kPa^{-1})		KIE
				Measured	Estimated[b]	
CO_2	4.0	0.20	105	3.8×10^5	5.5×10^3	1.62
H_2O	4.1	0.20	102	2.5×10^5	5.5×10^3	1.66
None	3.8[a]	0.19	99	1.6×10^5	5.5×10^3	1.71

[a] Initial CH_4 turnover rate on Ni surface.
[b] Calculated based on transition-state theory treatments of CH_4 activation steps proceeding via an immobile activated complex [59].

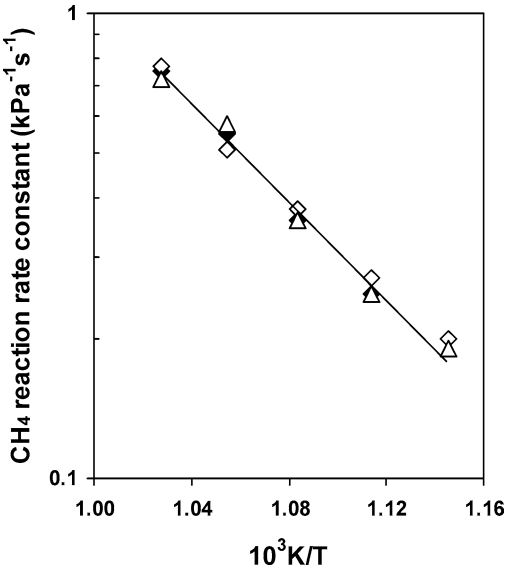

Fig. 8. Arrhenius plots for CO_2 reforming (◆), H_2O reforming (◇), and CH_4 decomposition (△) rate constants on 7 wt% Ni/MgO-A.

on 7 wt% Ni/MgO-A for H_2O (k_{H_2O}) and CO_2 (k_{CO_2}) reforming and CH_4 decomposition (k_{CH_4}) in this temperature range (Fig. 8) indicate that activation energies must also be similar for these three CH_4 reactions (Table 3) and that coreactants are required by stoichiometry, but they do not influence the dynamics of CH_4-reforming reactions. It appears that previous complex and contradictory rate equations may reflect varying and unrecognized contributions from concentration and temperature gradients or nonrigorous corrections for thermodynamic constraints.

The activation energies measured for first-order rate constants for CO_2 reforming (105 kJ/mol), H_2O reforming (102 kJ/mol), and CH_4 decomposition (99 kJ/mol) resemble those previously reported for CO_2 reforming (e.g., 92, 96, and 109 kJ/mol on Ni/MgO, Ni/SiO_2, and Ni/TiO_2) [44] and H_2O reforming (95 kJ/mol on Ni/Y-ZrO_2 [45]) on Ni catalysts and lie within a broad range of values reported for Ni supported on Al_2O_3 (74–118 kJ/mol [46–49]) and modified Al_2O_3 (90–107 kJ/mol [17,50]). Density-functional theory led to activation energy estimates of 85 kJ/mol [51], 93 kJ/mol [52], and 100 kJ/mol [53] for C–H bond activation of CH_4 on Ni(111) surfaces, while embedding methods led to slightly lower values (72 kJ/mol [54]). These theoretical estimates are in reasonable agreement with experiment and consistent with the conclusion that the dynamics of CH_4 reforming and decomposition reflect only the rate constants for C–H bond activation elementary steps on Ni surfaces.

These experimental and theoretical activation energies are, however, much greater than those measured for CH_4 activation on Ni single crystals [55–58]. Molecular beam studies led to activation energies of 52 kJ/mol [55] and 59 kJ/mol [56] on Ni(100). CH_4 dissociation rates at 0.13 kPa and 450–600 K, from chemisorbed carbon measured by Auger electron spectroscopy, gave activation energies of 52.7, 26.8, and 55.6 kJ/mol on Ni(111), Ni(100), and Ni(110), respectively [57,58].

It is possible that dissolved or chemisorbed carbon species form during initial contact with reactants in catalytic reactions and titrate those sites with the highest carbon binding energy, which would also dissociate C–H bonds most effectively by stabilizing the required transition state. It is unclear, however, why such passivation effects would not also influence reaction rates on model surfaces. Similar discrepancies between activation energies measured on catalysts and model surfaces were observed on Rh [31], Pt [32], and Ir [33], for which CO oxidation rates before and after reforming reactions showed that the number of available surface metal atoms remained unchanged during CH_4-reforming reactions. Any unreactive carbon species that formed on Ni surfaces during initial contact with reactants must be unreactive, because their concentration and therefore reforming rates would otherwise depend on the concentration and identity of coreactants. The reasons for these differences between steady-state catalytic rates on supported Ni clusters and rates estimated from C–H bond activation kinetic parameters on single crystals remain unclear, but may reflect the presence of specific defect sites on single crystals or the nature of the molecular beam experiments conducted on lower temperature surfaces.

Measured preexponential factors for CH_4 activation steps involved in CH_4–CO_2, CH_4–H_2O, and CH_4 decomposition reactions are about 100 times greater than predicted from transition-state theory for immobile activated complexes (Table 3). These differences suggest that activated complexes can undergo limited two-dimensional translation in the time scale of C–H bond activation events at typical reaction temperatures. Significant surface coverages by unreactive chemisorbed carbon species would have led instead to smaller than predicted preexponential factors.

Catalytic reactions of CH_4 with H_2O or CO_2 to form H_2–CO mixtures and stoichiometric CH_4 decomposition to form C^* and H_2 on Ni appear to depend only on the rate of initial activation of C–H bonds catalyzed by surface Ni atoms. Coreactant activation is facile and CH_4-derived intermediates, including reactive chemisorbed carbon, are kept well below monolayer coverages by their rapid reactions with intermediates derived from CO_2 or H_2O coreactants. In the next section, we describe kinetic isotope effect (KIE) data that confirm the exclusive kinetic relevance of C–H bond activation steps in CH_4–H_2O, CH_4–CO_2, and CH_4 decomposition reactions on Ni/MgO.

3.3. CH_4/CD_4 kinetic isotopic effects

Kinetic isotope effects on 7 wt% Ni/MgO-A were measured for CO_2 reforming from forward rates of CH_4–CO_2 and CD_4–CO_2 mixtures at 873 K, 25 kPa methane, and 25 kPa CO_2. For H_2O reforming, isotopic effects were measured from the corresponding forward rates for CH_4–H_2O, CD_4–H_2O, or CD_4–D_2O reactants at 873 K, 25 kPa

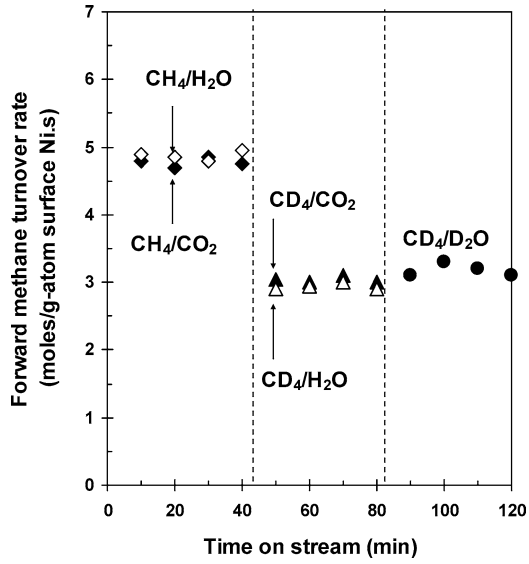

Fig. 9. Forward CH_4 reaction rates with CH_4/CO_2 (◆), CD_4/CO_2 (▲), CH_4/H_2O (◇), CD_4/H_2O (△), and CD_4/D_2O (●) reactant mixtures on 7 wt% Ni/MgO-A (5 mg catalyst, 873 K, 25 kPa CO_2 or H_2O, 25 kPa CH_4 or CD_4, 100 kPa total pressure, balance Ar).

methane, and 25 kPa water. Both CH_4–CO_2 and CH_4–H_2O reactions showed normal kinetic isotopic effects (Fig. 9) and these kinetic isotopic effects were identical for the two coreactants within experimental accuracy (Table 3). Forward rates were similar within experimental accuracy for CD_4–H_2O and CD_4–D_2O reactants (Fig. 9), indicating that neither water activation nor any steps involving adsorbed species derived from water are kinetically relevant. Kinetic isotope effects measured from initial CH_4 and CD_4 decomposition rates resemble those for catalytic CO_2 and H_2O-reforming reactions (Table 2), consistent with the equivalent rate-controlling steps proposed for the three reactions.

These isotope effects are very similar to those reported previously for CH_4 decomposition at 773 K on Ni/SiO_2 (1.60) [60] and for CO_2 reforming at 873 K on Ni/Al_2O_3 (1.45) [61]; they also resemble values we have recently reported on Ru (1.40–1.51) [31], Pt (1.58–1.77) [32], Ir (1.70–1.81) [33], and Rh (1.54–1.60) [34] at 873 K. On these noble metals, we also observed similar kinetic isotope effects for H_2O reforming, CO_2 reforming, and CH_4 decomposition. Some previous studies have reported similar CO_2-reforming rates with CH_4 and CD_4 reactants on Ni–La_2O_3 and Ni/SiO_2 and proposed the significant involvement of CO_2 activation and of chemisorbed oxygen in kinetically relevant steps [62–65]. These previous isotopic measurements were carried out at near-equilibrium conversions; their interpretation is inconsistent with the measured first-order dependence in CH_4, with the kinetic irrelevance of coreactant activation, and with the isotope effects reported here on Ni/MgO. They are likely to reflect isotope effects on equilibrium conversions, which are expected to be much smaller than isotopic effects on reaction rates.

Similar H_2O–CH_4-reforming and CH_4 decomposition rates on Ni foil at 1073 K led previous studies to conclude that only C–H bond activation steps limit overall H_2O-reforming rates [12], as also previously proposed for CO_2 reforming on Ni/Al_2O_3 without direct or specific evidence [15]. These conclusions are similar to those we reach here on the basis of more extensive experimental evidence. Several other studies, however, have reported markedly different conclusions. The kinetic misinterpretation of thermodynamic isotope effects led previous studies to conclude that CO_2 activation or reaction of chemisorbed carbon with oxygen limited overall reforming rates [63]. CO_2 dissociation [66] or its reaction with adsorbed CH_x species [61] was proposed to limit CO_2-reforming rates. A kinetic analysis [67] led one study to conclude that CH_4 dissociation can be reversible (a rigorous requirement as overall reactions approach equilibrium), that more than one elementary step limited overall rates, and that chemisorbed oxygen was involved in one or more of these limiting steps.

We note that the kinetic equivalence among CH_4 reactions, the specific dependence of rates on CH_4 and coreactant pressures, and the kinetic isotope effects reported here support the exclusive kinetic relevance of C–H bond activation and the lack of involvement of any species derived from coreactants in rate-limiting steps during either CH_4–H_2O or CH_4–CO_2 reactions. In the next sections, we provide additional isotopic evidence for the reversibility and kinetic relevance of several of the proposed elementary steps involved in these reactions.

3.4. Isotopic tracer studies of the reversibility of C–H bond activation

If C–H bond activation is the only kinetically relevant step, it must be exactly as reversible as the overall CH_4-reforming reaction, because the reaction affinity must be identical for the overall reaction and for the rate-determining step [41]. The reversibility of C–H bond activation can be measured from the rate of isotopic cross-exchange during $CH_4/CD_4/CO_2$ reactions. Reversible C–H bond activation steps would rapidly form CH_xD_{4-x} $(0 < x < 4)$ isotopomers via the microscopic reverse of C–H bond activation steps; in contrast, methane isotopomers would form much more slowly than chemical conversion products when C–H bond activation steps are irreversible.

$CH_4/CD_4/CO_2$ (1:1:2) mixtures were reacted on 7 wt% Ni/MgO-A at 873, 923, and 973 K and chemical and isotopic conversion rates were measured by on-line mass spectrometry after removing $H_xD_{2-x}O$ at 218 K to avoid interference among mass fragments for H_2O, HDO, D_2O species, and deuterated methane isotopomers. CH_4/CD_4 cross-exchange turnover rates, defined as the sum of the rates of formation of CHD_3, CH_2D_2 (taken twice), and CH_3D, are compared with chemical conversion turnover rates in Table 4. At 923 K, the methane chemical conversion rate is 8.8 s^{-1}, about 17 times greater than the isotopic cross-exchange rate. The ap-

Table 4
Methane chemical conversion rate and CH_4/CD_4 cross-exchange rate during $CH_4/CD_4/CO_2$ reaction on 7 wt% Ni/MgO (12.5 kPa CH_4 and CD_4, 25 kPa CO_2, 100 kPa total pressure, balance Ar)

Reaction temperature (K)	Methane chemical conversion turnover rate (s^{-1})[a]	Cross exchange rate (s^{-1})[b]	$r_{exch}/r_{reaction}$[c]	η[d]
873	3.5	0.24	0.07	0.06
923	8.8	0.50	0.06	0.05
973	19.0	0.85	0.04	0.05

[a] Forward methane chemical conversion rate.
[b] Total methane isotopomers formation rate.
[c] Ratio of total methane isotopomers formation rate to the methane chemical conversion rate.
[d] $\eta = ([P_{CO}]^2[P_{H_2}]^2)/([P_{CO_2}][P_{CH_4}]K)$; approach to equilibrium for CO_2-reforming reaction.

proach to equilibrium for this reaction, η, estimated from the prevalent concentrations of all reactants and products is 0.05, corresponding to the ratio of the forward reaction rate to the reverse reaction rate of 20, indicating that CHD_3, CH_2D_2, and CH_3D isotopomers formed merely because the overall reaction is reversible to some extent under the conditions of the experiment. These data show that C–H bond activation steps are exactly as reversible as the overall CH_4–CO_2 reaction, as required by their rate-determining nature. These results and conclusions resemble those obtained from similar experiments on Ru [31], Pt [32], Ir [33], and Rh [34]. Other studies [24,65,68] have assumed, without specific evidence, that C–H bond activation is reversible during CO_2 reforming. CO_2 reforming [68] and partial oxidation [69] of CH_4/CD_4 mixtures on Ni/SiO_2 showed that C–H bond activation was reversible and that chemical conversion and CH_xD_{4-x} formation rates were similar, a conclusion that merely indicates that the overall reaction was reversible at the high chemical conversions inappropriately used in these measurements (e.g., 84.7% at 973 K for CO_2 reforming [68]).

The H/D ratio in the dihydrogen formed during CO_2 reforming of equimolar CH_4–CD_4 mixtures on 7 wt% Ni/MgO-A at 873 K is 1.56. These data confirm the higher reactivity of CH_4 relative to CD_4 and the kinetic isotope effect values measured from independent CH_4–CO_2 and CD_4–CO_2 reactants (1.62). Dihydrogen molecules showed a binomial isotopomer distribution, indicating that recombinative hydrogen desorption steps are quasi-equilibrated, a conclusion confirmed by the isotopic data presented next.

3.5. Isotopic probes of the reversibility of hydrogen and hydroxyl recombination steps that form H_2 and H_2O

Some water forms during CO_2 reforming of CH_4 because chemisorbed hydrogen (from CH_4) reacts with chemisorbed oxygen (from CO_2) in an overall reaction that mimics the stoichiometry of the reverse water–gas shift. This reaction and therefore all elementary steps required are quasi-equilibrated during CH_4 reforming with H_2O or CO_2, as shown from the effluent concentrations measured under all reaction conditions (Fig. 10). Thus, we expect that formation

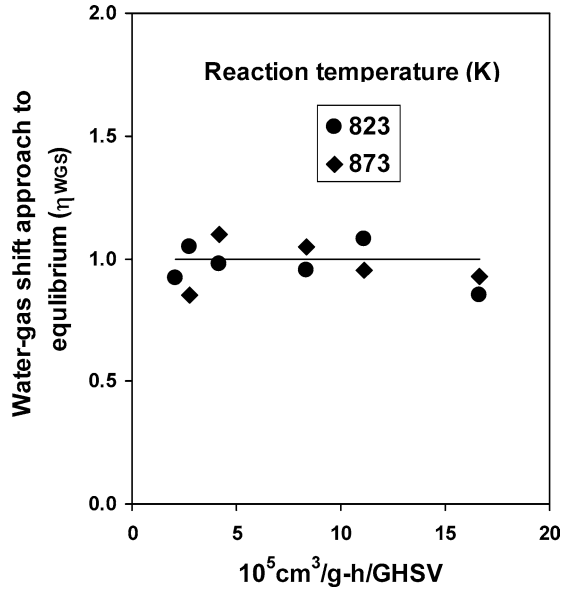

Fig. 10. Extent of water–gas-shift equilibration at different reaction temperatures as a function of space velocity on 7 wt% Ni/MgO-A (25 kPa CH_4, 25 kPa CO_2, 100 kPa total pressure, balance He, $\eta_{WGS} = ([P_{CO}][P_{H_2O}])/([P_{H_2}][P_{CO_2}]K_{WGS}))$.

and desorption of water occur via quasi-equilibrated elementary steps.

Dihydrogen and water isotopomers were measured by online mass spectrometry during reactions of $CH_4/CO_2/D_2$ (1:1:0.2) mixtures on 7 wt% Ni/MgO-A at 973 K. The H/D fraction expected if all H atoms in chemically converted CH_4 molecules and all D atoms in D_2 molecules contributed to the pool of surface intermediates forming water and dihydrogen is 3.81. Measured H/D ratios in water and dihydrogen molecules formed during $CH_4/CO_2/D_2$ reaction were 3.66 and 3.90, respectively. Thus, complete equilibration occurs between dihydrogen and water molecules and their respective chemisorbed precursors. Isotopomer distributions for both water and dihydrogen were binomial (Fig. 11), consistent with quasi-equilibrated recombination steps involving H^* and OH^* to form water and H^* and H^* to form dihydrogen. The quasi-equilibrated nature of the steps forming water and dihydrogen, the rapid isotopic equilibration of CO–CO_2 mixtures discussed below, and the expected equilibrium for molecular adsorption of CO under these conditions would require that water–gas-shift reactions also be at

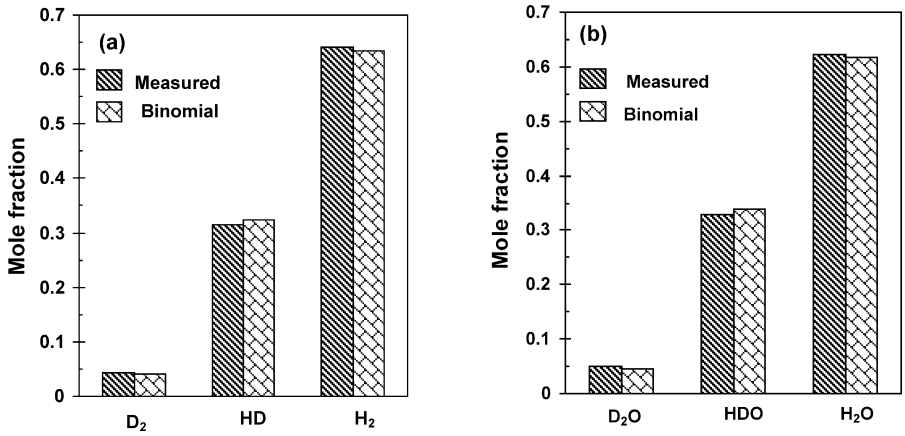

Fig. 11. Distribution of dihydrogen (a) and water (b) isotopomers during reactions of $CH_4/CO_2/D_2$ mixtures on 7 wt% Ni/MgO-A (973 K, 16.7 kPa CH_4, 16.7 kPa CO_2, 3.3 kPa D_2, 100 kPa total pressure, balance Ar).

equilibrium during CO_2 and H_2O reforming on Ni catalysts, as indeed found under all reaction conditions in this study (Fig. 10).

3.6. Isotopic probes of reversible coreactant activation steps

The reversibility of CO_2 activation steps during CO_2–CH_4 reactions was probed using $^{12}CH_4/^{12}CO_2/^{13}CO$ (1:1:0.4) reactant mixtures on 7 wt% Ni/MgO-A at 973 K. Measured ^{13}C fractions were very similar in CO (0.24) and CO_2 (0.23) molecules leaving the catalyst bed, even when the overall reforming reaction was far from equilibrium ($\eta = 0.06$). These ^{13}C contents reflect complete chemical and isotopic equilibration between CO and CO_2 molecules in the contacting gas phase; they confirm that CO_2 activation steps are much faster than kinetically relevant C–H bond activation steps, and that CO_2 dissociation to CO and oxygen occurs in both directions many times during each CH_4 chemical conversion turnover. CO_2 activation steps are reversible and quasi-equilibrated during CH_4–CO_2 reactions and we conclude from kinetic analogies with CH_4–H_2O reactions that H_2O activation steps are also reversible and quasi-equilibrated during the latter reaction. This conclusion is consistent with the equilibrated nature of water–gas-shift reactions during steam reforming; it will be confirmed in future studies via ^{18}O isotopic tracing using $CH_4/H_2{}^{18}O/C^{16}O$ reactants.

3.7. Elementary steps involved in CH_4-reforming reactions

These isotopic tracing and exchange measurements confirmed the mechanism first proposed based on measured kinetic effects of reactant and product concentrations of forward reaction rates. The sole kinetic relevance of CH_4 activation is consistent with the results of $CH_4/CO_2/D_2$, $CH_4/CD_4/CO_2$, and $^{12}CH_4/^{12}CO_2/^{13}CO$ reactions. The quasi-equilibrated nature of CO_2 activation was confirmed by the similar ^{13}C fraction in CO and CO_2 during $^{12}CH_4/^{12}CO_2/^{13}CO$ reactions. H_2 and H_2O form in quasi-equilibrated steps.

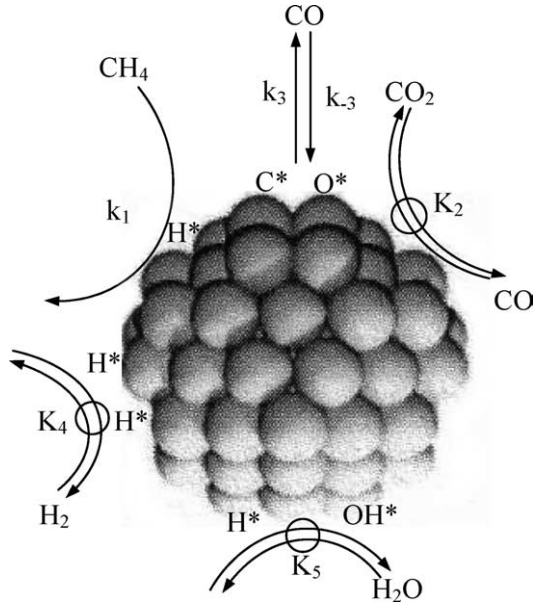

Scheme 1. Sequence of elementary steps for CH_4-reforming and water–gas-shift reactions on Ni-based catalysts ($\rightarrow$ irreversible step, $\leftrightarrows$ quasi-equilibrated step, $\rightleftarrows$ reversible step, k_i is the rate coefficient and K_i is the equilibrium constant for a given step i).

This evidence led us to consider the sequence of elementary steps shown in Scheme 1, which accounts for H_2O and CO_2 reforming, CH_4 decomposition, and water–gas-shift reactions and also provides steps required to form chemisorbed carbon precursors to carbon filaments. CH_4 decomposes to chemisorbed carbon (C^*) via sequential elementary H-abstraction steps, which become faster as H atoms are sequentially abstracted from CH_4 reactants. Density-functional theory led to an activation energy of 142 kJ/mol for the first H-abstraction step in CH_4 on Ni clusters, which decreased to 25–40 kJ/mol for CH_2 formation from CH_3 [70]. This cascade process leads to low

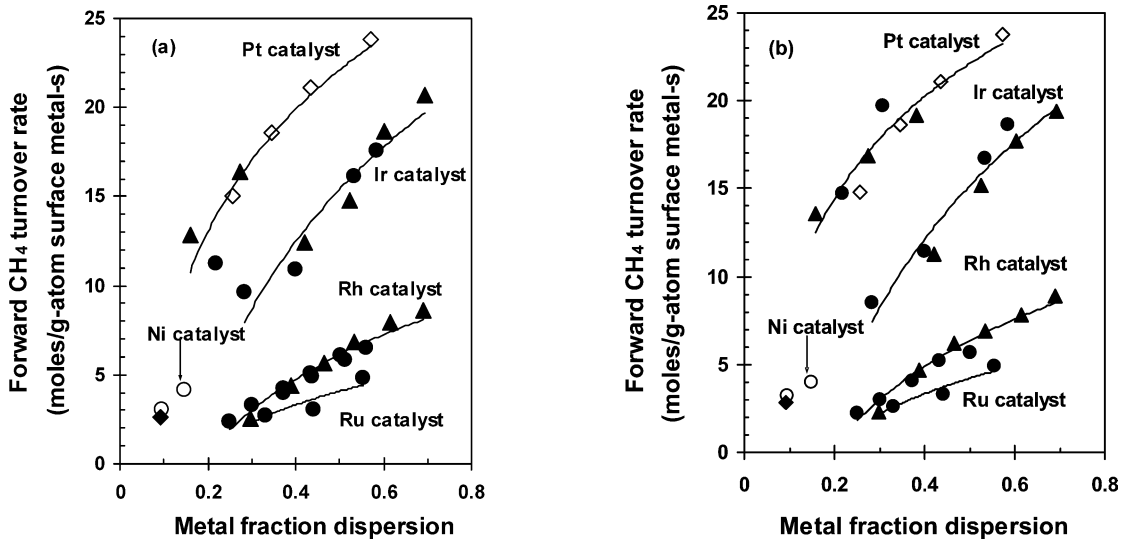

Fig. 12. Forward CH_4 turnover rates for CO_2 (a) and H_2O (b) reforming of CH_4 on different metal clusters as a function of metal dispersion on various supports (873 K, 20 kPa CH_4, (▲) ZrO_2, (●) γ-Al_2O_3, (◇) ZrO_2–CeO_2 as support, (○) MgO-A, (◆) MgO-B).

$CH_x{}^*$ coverages and to C^* as the most abundant carbon-containing reactive intermediate. Chemisorbed carbon is then removed using CO_2 or H_2O as coreactants. These elementary steps are consistent also with kinetic and isotopic measurements on Ru [31], Pt [26], Ir [32], and Rh [33] catalysts. When exposed metal atoms (*) are the most abundant surface species, only the rate constant for the activation of the first C–H bond in CH_4 appears in the rate expression and reaction rates become first order in CH_4 and independent of the presence or concentration of CO_2 or H_2O coreactants. We note that these elementary steps provide pathways for reactions of CH_4 with either CO_2 or H_2O and also for water–gas-shift reactions ($H_2O + CO \overset{K_{WGS}}{\rightleftharpoons} CO_2 + H_2$), which have been typically, but inappropriately and nonrigorously, treated as independent kinetic processes during CH_4 reforming.

The general features of this sequence are in essential agreement with previous mechanistic proposals on supported Ni catalysts [21,59,71] and supported noble catalysts [72,73], which lacked steps required for complete water–gas-shift sequences and which did not provide direct evidence for the reversibility of the elementary steps [21,59]. It appears that some accumulation of unreactive carbon in some of these previous studies, possibly as a result of transport restrictions, led to the incorrect conclusion that reactions between chemisorbed carbon and oxygen limit CO_2-reforming rates on Ni surfaces [21].

Detailed kinetic and isotopic tracer studies of CH_4–H_2O, CH_4–CO_2, and CH_4 decomposition and water–gas-shift reactions on noble metals (Rh, Ru, Pt, Ir) have been reported elsewhere [31–34]. These studies also provided kinetic and isotopic evidence for the identity and reversibility of elementary steps involved in CH_4-reforming reactions and for the sole kinetic relevance of C–H bond activation and mechanism equivalence among CH_4-reforming and decomposition reactions. Next, we compare measured C–H bond activation turnover rates on noble metal (Rh, Ru, Pt, Ir) and Ni catalysts.

3.8. Effect of the identity of metal clusters on C–H bond activation

Metal dispersion and support effects on forward CH_4 turnover rates for CH_4–H_2O, CH_4–CO_2, and CH_4 decomposition reactions were reported earlier on individual noble metal catalysts (Rh, Ru, Pt, Ir) [31–34]. For each noble metal, CH_4-reforming turnover rates (normalized by exposed metal atoms and corrected by their approach to equilibrium) increased with increasing metal dispersion, but they were not influenced by the support (Al_2O_3, ZrO_2, and ZrO_2–CeO_2) [31–34]. The demonstrated kinetic irrelevance of coreactant activation implies that even when supports catalyze coreactant activation, they cannot influence overall reaction rates.

Fig. 12 shows forward CH_4-reforming turnover rates with CO_2 (Fig. 12a) and H_2O (Fig. 12b) on supported Pt, Ir, Rh, and Ru catalysts with a relatively wide dispersion range and on the three Ni catalysts of this study. The exclusion of transport and thermodynamic artifacts, the rigorous correction to the forward rates, and the measurement of rates normalized by the relevant exposed surface metal atoms make these rate comparisons a rigorous reflection of the kinetic reactivity of such metal surfaces. One previous comparison of reactivity was based on CH_4 conversion during CO_2 reforming for various metals on Al_2O_3 supports, but neither metal dispersions nor turnover rates were reported [74]. Another study compared CH_4 turnover rates on noble metals supported on Al_2O_3–MgO and observed a reactivity order (Ru > Rh > Ir > Ni > Pt) [75], very different from the order reported here for both CO_2–CH_4 and H_2O–CH_4 reac-

tions. These differences arise, at least in part, from dispersion differences among the noble metal catalysts compared in Ref. [75], which lead to marked differences in reactivity (Fig. 12), and to varying approaches to equilibrium at the different CH_4 conversions used in this previous comparison. The data shown in Fig. 12 appear to be the first rigorous comparison of the C–H bond activation rates on supported noble metal and Ni clusters over a common dispersion range. Among these different metal clusters, Pt clusters show the most reactive surfaces for C–H bond activation.

3.9. Mechanistic implications for the dynamics of carbon filament formation during CH_4 reforming and decomposition

Here, we discuss briefly the implications of the proposed CH_4 reaction mechanism for kinetic treatments of filamentous carbon formation. All rate constants and steps refer to those in the Scheme 1. The concentration (C^*) or thermodynamic activity (a_{C^*}) of chemisorbed carbon depends on prevalent pressures and on the rate and equilibrium constants for individual elementary steps. A pseudo-steady-state analysis based on C^* and * as the most abundant reactive intermediates gives

$$a_{C^*} = k_c\left[\frac{k_1 P_{CH_4}}{K_2 k_3 K_4 P_{CO_2}} + \frac{k_{-3} P_{CO}}{K_2 k_3 K_4 P_{CO_2}}\right] P_{CO}. \tag{7}$$

When carbon removal by surface oxygen step ($C^* + O^* \overset{k_3}{\underset{k_{-3}}{\leftrightarrows}} CO^* + {}^*$) is quasi-equilibrated,

$$k_{-3}(CO) \ll k_1(CH_4), \tag{8}$$

Eq. (7) becomes

$$a_{C^*} = \frac{k_c k_1 P_{CH_4} P_{CO}}{K_2 k_3 K_4 P_{CO_2}} = \frac{k P_{CH_4} P_{CO}}{P_{CO_2}} \tag{9}$$

or

$$a_{C^*} = \frac{k P_{CH_4} P_{H_2}}{K_{WGS} P_{H_2O}} = \frac{k' P_{CH_4} P_{H_2}}{P_{H_2O}}, \tag{10}$$

in which $P_{CH_4}P_{CO}/P_{CO_2}$ and $P_{CH_4}P_{H_2}/P_{H_2O}$ are related to each other by the water–gas-shift equilibrium constant; thus, these two ratios are proportional to each other at each given temperature. The thermodynamic carbon activity (a_{C^*}) that provides the driving force for carbon filament formation is proportional to $P_{CH_4}P_{CO}/P_{CO_2}$ (or equivalently $P_{CH_4}P_{H_2}/P_{H_2O}$).

Fig. 13 shows carbon formation rates as a function of these two ratios, which were varied by changing CH_4, CO_2, or H_2O partial pressures or the space velocity, as well as by adding H_2 during CH_4–CO_2 reactions at 873 K on Ni/MgO-A and Ni/MgO-B catalysts. For $P_{CH_4}P_{CO}/P_{CO_2}$ ratios in the range of 1.1–4.5 kPa ($P_{CH_4}P_{H_2}/P_{H_2O} \sim 2.7$–11.0 kPa), carbon formation rates increased linearly with increasing carbon activity on 7 wt% Ni/MgO-A, irrespective of how these ratios were varied (e.g., residence time, CH_4 pressure, CO_2 or H_2O pressure, H_2 addition). Electron microscopy detected the formation of hollow multiwalled carbon nanotubes with diameters similar to those of the Ni crystallites attached to their advancing tips. Comparing the carbon formation rate on Ni/MgO-A and Ni/MgO-B, we found that for a given value of $P_{CH_4}P_{CO}/P_{CO_2}$ or $P_{CH_4}P_{H_2}/P_{H_2O}$, carbon formation rates (per surface Ni atom) increase with increasing Ni crystallite diameter, apparently as a result of the more facile nucleation and lower thermodynamic carbon activity for the larger carbon filaments prevalent in such larger crystallites.

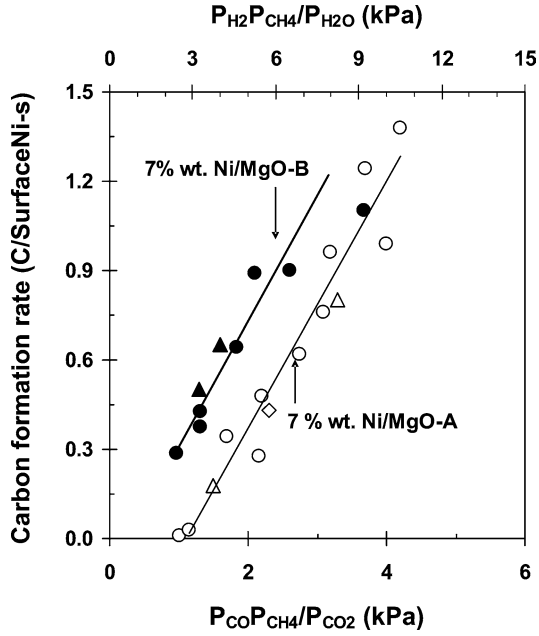

Fig. 13. Effect of $P_{CO}P_{CH_4}/P_{CO_2}$ or $P_{H_2}P_{CH_4}/P_{H_2O}$ on carbon formation rate on Ni/MgO-A and Ni/MgO-B at 873 K ($P_{CO}P_{CH_4}/P_{CO_2}$ or $P_{H_2}P_{CH_4}/P_{H_2O}$ ratios were changed by varying CH_4 and CO_2 or H_2O partial pressures or space velocity during CH_4/CO_2 and CH_4/H_2O reactions. (○,●) CH_4/CO_2 reaction, (△,▲) CH_4/H_2O reaction, and (◇) addition of H_2 in CH_4/CO_2 reaction).

The observed linear dependence of carbon formation rates on these two parameters is consistent with diffusion-limited growth of filaments driven by a gradient in activity between the exposed Ni surface and the carbon filament [76,77], which increases as $P_{CH_4}P_{CO}/P_{CO_2}$ or $P_{CH_4}P_{H_2}/P_{H_2O}$ increases. The rate of carbon formation for a given value of $P_{CH_4}P_{CO}/P_{CO_2}$ or $P_{CH_4}P_{H_2}/P_{H_2O}$ increased with increasing Ni particle size, even though exposed Ni surface areas are lower and carbon must diffuse through larger Ni crystallites. These effects of crystallite size appear to reflect the lower carbon activity required to nucleate large filaments (the x intercept in Fig. 13) and the temperature dependence of the groupings of kinetic and thermodynamic constants that relate $P_{CH_4}P_{CO}/P_{CO_2}$ and $P_{CH_4}P_{H_2}/P_{H_2O}$ to the carbon thermodynamic activity. A more detailed treatment of filament formation rate and of parallel mechanisms for catalyst deactivation via encapsulation of Ni particles will be reported elsewhere [35].

4. Conclusions

Isotopic studies and forward rate measurements led to a simple and comprehensive mechanistic picture for CH_4–CO_2 and CH_4–H_2O reforming, CH_4 decomposition, and water–gas-shift reactions on Ni-based catalysts. The mechanistic equivalence among CH_4-reforming and decomposition reactions was confirmed by identical forward CH_4 reaction rates, rate constants, kinetic isotopic effect, and activation energies measurements for the three CH_4 reactions. CH_4 reaction rates were limited solely by C–H bond activation steps and unaffected by the identity or concentration of coreactants. Isotopic tracer and exchange studies confirmed that C–H bond activation is the only kinetically relevant step and that it is exactly as reversible as the overall reforming reaction. Isotopic evidence also showed that activation of H_2, CO_2, and H_2O was reversible and quasi-equilibrated during CO_2 and H_2O-reforming reactions of CH_4. The rigorous exclusion of transport artifacts and the accurate correction of net rates for thermodynamic constraints led to the first comparison of true turnover rates among Ni and noble metal catalysts. The elementary steps proposed and confirmed by kinetic and isotopic evidence provide a rigorous basis for treating the dynamics of carbon formation during CH_4 reforming. The thermodynamic activity of chemisorbed carbon species, which provides the kinetic driving force for filament formation, and the rate of carbon formation depend linearly on the prevalent $P_{CH_4}P_{CO}/P_{CO_2}$ (or $P_{CH_4}P_{H_2}/P_{H_2O}$) ratios in the contacting gas phase.

Acknowledgments

This study was supported by BP as part of the Methane Conversion Cooperative Research Program at the University of California. Helpful technical discussions with Drs. John Collins and Theo Fleisch (BP) throughout these studies are gratefully acknowledged.

References

[1] V.F. Fischer, H. Tropsch, Brennstoff-Chemie 3 (1928) 39–46.
[2] J.H. Edwards, A.M. Maitra, Fuel Process. Technol. 42 (1995) 269.
[3] S.B. Wang, G.Q. Lu, Energy Fuels 10 (1996) 896.
[4] M.C.J. Bradford, M.A. Vannice, Catal. Rev.-Sci. Eng. 41 (1999) 1.
[5] J.W. Snoeck, G.F. Froment, Ind. Eng. Chem. Res. 41 (2002) 3548.
[6] H.S. Bengarrd, J.K. Norskov, J. Sehested, B.S. Clause, L.P. Nielsen, A.M. Molenbroek, J.R. Rostrup-Nielsen, J. Catal. 209 (2002) 365.
[7] D.E. Resasco, W.E. Alvarez, F. Pompeo, L. Balzano, J.E. Herrera, B. Kitiyanan, A. Borgna, J. Nano. Res. 4 (2002) 131.
[8] W.W. Akres, D.P. Camp, AIChE J. 1 (1955) 471.
[9] N.M. Bodrov, L.O. Apel'baum, Kinet. Katal. 5 (1964) 614.
[10] N.M. Bodrov, L.O. Apel'baum, M.I. Temkin, Kinet. Katal. 8 (1967) 821.
[11] T.Q.P. Quach, D.J. Rouleau, Appl. Chem. Biotechnol. 25 (1975) 445.
[12] P. Munster, H.J. Grabke, J. Catal. 72 (1981) 279.
[13] J. Xu, G.F. Froment, AIChE J. 35 (1989) 88.
[14] J. Xu, G.F. Froment, AIChE J. 35 (1989) 97.
[15] Z.L. Zhang, X.E. Verykios, Catal. Today 21 (1994) 589.
[16] M.C.J. Bradford, M.A. Vannice, Appl. Catal. A 142 (1996) 97.
[17] U. Olsbye, T. Wurzel, L. Mleczko, Ind. Eng. Chem. Res. 36 (1997) 5180.
[18] T. Osaki, T. Horuchi, K. Suzuki, T. Mori, Appl. Catal. A 155 (1997) 229.
[19] V.C.H. Kroll, G.J. Tjatjopoulos, C. Mirodatos, Stud. Surf. Sci. Catal. 119 (1998) 753.
[20] S. Wang, G.Q. Lu, React. Eng. Pollut. Prev. (2000) 75.
[21] S. Bebelis, A. Zeritis, C. Tiropani, S.G. Neophytides, Ind. Eng. Chem. Res. 39 (2000) 4920.
[22] K. Hou, R. Hughes, Chem. Eng. J. 82 (2001) 311.
[23] V.A. Tsipouriari, X.E. Verykios, Catal. Today 64 (2001) 83.
[24] A. Becerra, M.E. Iriarte, A.E. Castro-Luna, React. Kinet. Catal. Lett. 79 (2003) 119.
[25] R.W. Stevens, S.S.C. Chuang, J. Phys. Chem. B 108 (2004) 696.
[26] K. Takehira, T. Shishido, P. Wang, J. Catal. 221 (2004) 43.
[27] X.E. Verykios, Appl. Catal. A 255 (2003) 101.
[28] A. Shamsi, C.D. Johnson, Catal. Today 84 (2003) 17.
[29] Z. Chen, Y. Yan, S.S.E.H. Elnashaie, AIChE J. 49 (2003) 1250.
[30] M. Zanfir, A. Gavriilidis, Chem. Eng. Sci. 58 (2003) 3947.
[31] J. Wei, E. Iglesia, J. Phys. Chem. B, in press.
[32] J. Wei, E. Eglesia, J. Phys. Chem. B 108 (2004) 4094.
[33] J. Wei, E. Iglesia, Angew. Chem. Int. Edit., in press.
[34] J. Wei, E. Iglesia, J. Catal. (2004), in press.
[35] J. Wei, E. Iglesia, manuscript in preparation.
[36] K.S. Suslick, T. Hyeon, M. Tang, Chem. Mater. 8 (1996) 2172.
[37] G.L. Price, E. Iglesia, Ind. Eng. Chem. 28 (1989) 839.
[38] E. Ruckenstein, Y.H. Hu, Appl. Catal. A 154 (1997) 185.
[39] K. Tosishige, O. Yomazaki, Y. Chen, K. Yokoyama, X. Li, K. Fujimoto, Catal. Today 45 (1998) 35.
[40] D.R. Stull, F. Edgar, J. Westrum, G.C. Sinke, In the Thermodynamics of Organic Compounds, Krieger, Malabar, FL, 1987.
[41] M. Boudart, G. Djega-Mariadassou, The Kinetics of Heterogeneous Catalytic Reactions, Princeton Univ. Press, Princeton, NJ, 1984.
[42] A.J. Muscat, R.J. Madix, J. Phys. Chem. 100 (1996) 9807.
[43] K. Christmann, O. Schober, G. Ertl, M. Neumann, J. Chem. Phys. 60 (1974) 4528.
[44] M.C.J. Bradford, M.A. Vannice, Appl. Catal. A 142 (1996) 73.
[45] K. Ahmed, K. Foger, Catal. Today 63 (2000) 479.
[46] S. Wang, G. Lu, Energy Fuels 12 (1998) 248.
[47] L.M. Aparico, A.G. Ruiz, I.R. Ramoa, Appl. Catal. A 170 (1998) 177.
[48] O. Tokunaga, S. Ogasawara, React. Kinet. Catal. Lett. 39 (1989) 69.
[49] T. Horiuchi, K. Sakuma, T. Fukui, Y. Kubo, T. Osaki, T. Mori, Appl. Catal. A 144 (1996) 111.
[50] A.A. Lemonidou, L.A. Vasalos, Appl. Catal. A 228 (2002) 227.
[51] I.M. Ciobica, F. Frechard, R.A. van Santen, A.W. Kleyn, J. Hafner, J. Phys. Chem. B 104 (2000) 3364.
[52] A.P.J. Jansen, H. Burghgraef, Surf. Sci. 344 (1995) 149.
[53] P. Kratzer, B. Hammer, J.K. Norskov, J. Chem. Phys. 105 (1996) 5595.
[54] H. Yang, J.L. Whitten, J. Chem. Phys. 96 (1992) 5529.
[55] I. Chorkendorff, I. Alstruo, S. Ullmann, Surf. Sci. 227 (1990) 291.
[56] B. Olgaard Nielsen, A.C. Luntz, P.M. Holmblad, I. Chorkendorff, Catal. Lett. 32 (1995) 15.
[57] T.P. Beebe, D.W. Goodman, B.D. Kay, J.T. Yates, J. Chem. Phys. 87 (1987) 2305.
[58] X. Jiang, D.W. Goodman, Catal. Lett. 4 (1990) 173.
[59] J.A. Dumesic, D.F. Rudd, J.E. Rekoske, A.A. Trevino, The Microkinetics of Heterogeneous Catalysis, Am. Chem. Society, Washington, DC, 1993.
[60] K. Otsuka, S. Kobayashi, S. Takenaka, J. Catal. 200 (2001) 4.
[61] T. Osaki, T. Horiuchi, K. Suzuki, T. Mori, Catal. Lett. 44 (1997) 19.
[62] Y. Schuurman, V.C.H. Kroll, P. Ferreira-Aparicio, C. Mirodatos, Catal. Today 38 (1997) 129.
[63] V.C.H. Kroll, H.M. Swaan, S. Lacombe, C. Mirodatos, J. Catal. 164 (1997) 387.
[64] J. Chang, S. Park, J.W. Yoo, J. Park, J. Catal. 195 (2000) 1.

[65] S. Tang, L. Ji, J. Lin, H.C. Zeng, K.L. Tan, K. Li, J. Catal. 194 (2000) 424.
[66] J.J. Gamman, G.J. Millar, G. Rose, J. Drennan, J. Chem. Soc., Faraday Trans. 94 (1998) 701.
[67] L.M. Aparicio, J. Catal. 165 (1997) 262.
[68] V.C.H. Kroll, H.M. Swaan, C. Mirodatos, J. Catal. 161 (1996) 409.
[69] V.C.H. Kroll, P.S. Delichure, C. Mirodatos, Kinetic. Catal. 37 (1996) 698.
[70] H. Burghgraef, A.P.J. Jansen, R.A. van Santen, Surf. Sci. 324 (1995) 345.
[71] J.A. Lercher, J.H. Bitter, W. Hally, W. Niessen, K. Seshan, Stud. Surf. Sci. Catal. 101 (1996) 463.
[72] S.M. Stagg, Stud. Surf. Sci. Catal. 111 (1997) 543.
[73] A.M. O'Connor, F.C. Meunier, J.R.H. Ross, Stud. Surf. Sci. Catal. 119 (1998) 819.
[74] F. Solymosi, G. Kutsan, A. Erdohelyi, Catal. Lett. 11 (1991) 149.
[75] J.R. Rostrup-Nielsen, J.H. Bak Hansen, J. Catal. 144 (1993) 38.
[76] I. Alstrup, T. Tavares, C.A. Bernardo, O. Sorensen, J.R. Rostrup-Nielsen, Mater. Corrosion 49 (1998) 367.
[77] S.A. Safvi, E.C. Bianchini, C.R.F. Lund, Carbon 29 (1991) 1245.